

Nanodelivery of Mycophenolate Mofetil to the Organ Improves Transplant Vasculopathy

Mayuko Uehara,^{†,‡} Baharak Bahmani,^{†,‡} Liwei Jiang,^{†,‡} Sungwook Jung,[†] Naima Banouni,[†] Vivek Kasinath,[†] Zhabiz Solhjoui,[†] Jing Zhao,[†] Farideh Ordikhani,[†] Munhyung Bae,[‡] Nasim Annabi,^{§,Ⓛ} Martina M. McGrath,^{*,†} and Reza Abdi^{*,†,Ⓛ}

[†]Transplantation Research Center, Renal Division, Brigham and Women's Hospital, Harvard Medical School, Boston, Massachusetts 02115, United States

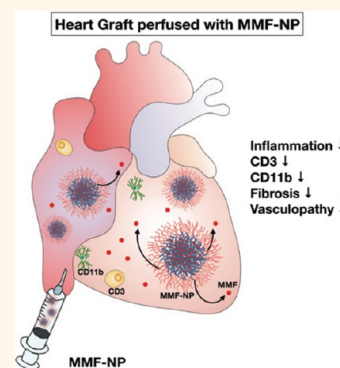
[‡]Department of Biological Chemistry and Molecular Pharmacology, Harvard Medical School, Boston, Massachusetts 02115, United States

[§]Department of Chemical and Biomolecular Engineering, University of California at Los Angeles, Los Angeles, California 90095-1592, United States

Supporting Information

ABSTRACT: Inflammation occurring within the transplanted organ from the time of harvest is an important stimulus of early alloimmune reactivity and promotes chronic allograft rejection. Chronic immune-mediated injury remains the primary obstacle to the long-term success of organ transplantation. However, organ transplantation represents a rare clinical setting in which the organ is accessible *ex vivo*, providing an opportunity to use nanotechnology to deliver therapeutics directly to the graft. This approach facilitates the directed delivery of immunosuppressive agents (ISA) to target local pathogenic immune responses prior to the transplantation. Here, we have developed a system of direct delivery and sustained release of mycophenolate mofetil (MMF) to treat the donor organ prior to transplantation. Perfusion of a donor mouse heart with MMF-loaded PEG–PLGA nanoparticles (MMF-NPs) prior to transplantation abrogated cardiac transplant vasculopathy by suppressing intragraft pro-inflammatory cytokines and chemokines. Our findings demonstrate that *ex vivo* delivery of an ISA to donor organs using a nanocarrier can serve as a clinically feasible approach to reduce transplant immunity.

KEYWORDS: nanodelivery, transplant, mycophenolate mofetil, chronic rejection, selective drug delivery



Solid organ transplantation has become a mainstay of treatment for patients with end-stage organ failure. Over the past decades, the use of increasingly potent immunosuppressive agents (ISAs) has reduced overall rates of acute transplant rejection and improved short-term graft survival. However, long-term transplant outcomes have failed to improve to the same degree.^{1,2} Furthermore, in addition to organ toxicity, ISAs are a significant contributor to several post-transplantation complications, including infection, cardiovascular disease, diabetes, and malignancy.^{3–5} Attempts to minimize ISAs, such as cyclosporine and tacrolimus, have had mixed success and are associated with increased risk of acute transplant rejection.^{3,6,7}

Inflammatory responses occurring within the allograft early in the post-transplantation period significantly enhance alloimmunity.^{8,9} Intragraft inflammation begins prior to organ procurement, when upregulation of inflammatory cytokines and adhesion molecules within donor organs occurs simultaneously with brain death.¹⁰ This process peaks in the postanastomosis period, coincident with extensive ischemia-

reperfusion injury (IRI). IRI leads to activation of intragraft antigen-presenting cells, including dendritic cells (DCs).^{11,12} DCs activated by intragraft inflammation, in turn, promote alloreactive T cell responses, enhancing chronic alloimmune injury.^{11–13} Therefore, the development of more effective strategies to control early immune-activating events within the organ and improve long-term transplant outcomes remains a major focus of investigation in transplantation.

Notable progress in synthesizing and characterizing nanoscale materials has sparked interest in refining the methods of drug delivery, especially in the field of oncology.^{14,15} Nanotechnology has been used to improve pharmacokinetic profiles, leading to controlled, sustained release of an agent and its delivery to the site of interest.^{16–20} In contrast to most models of systemic disease, transplantation is a unique scenario, in which the

Received: June 30, 2019

Accepted: September 13, 2019

Published: September 13, 2019

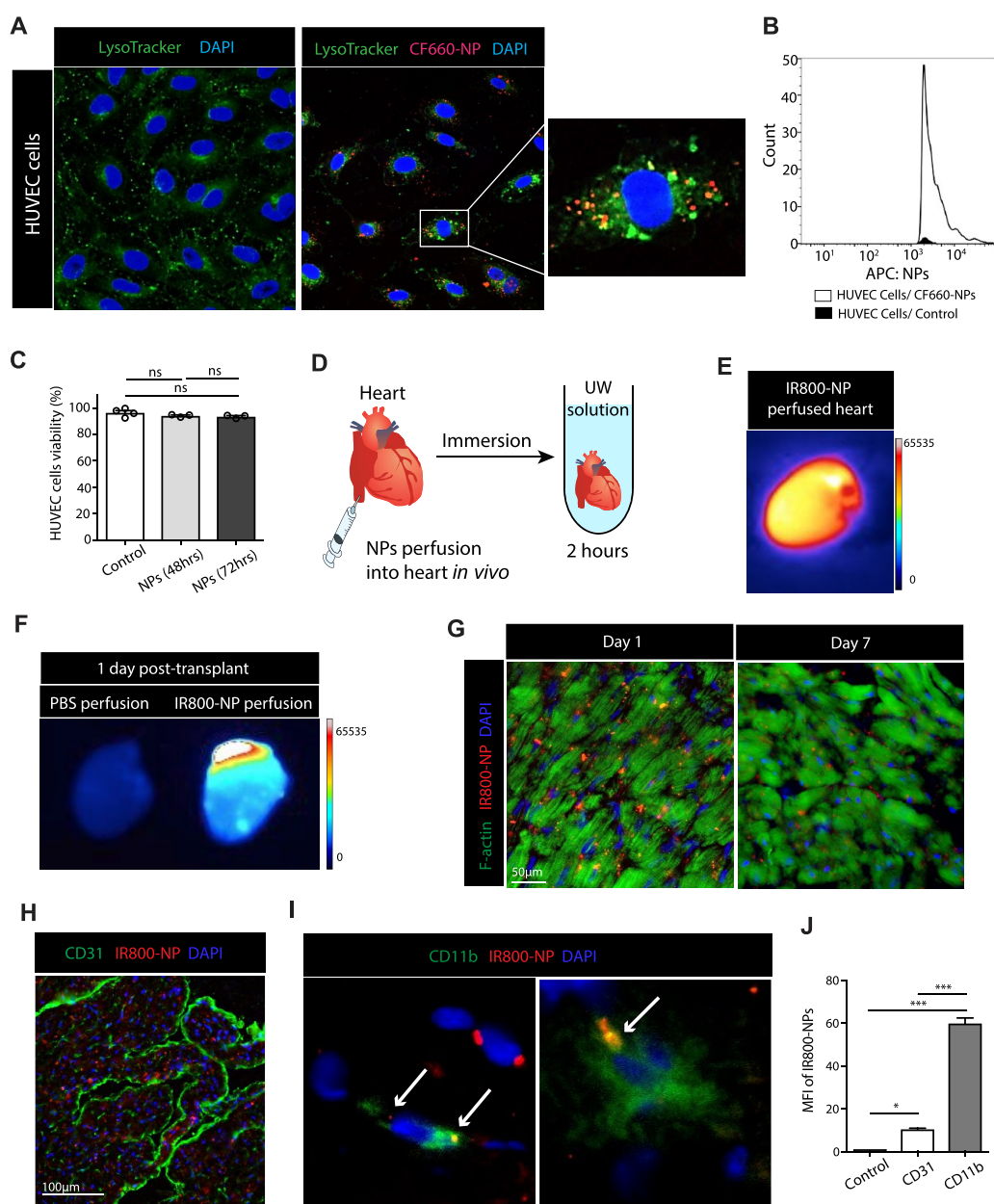


Figure 1. Cellular uptake and organ delivery of PEG–PLGA nanoparticles *in vivo* and *in vitro*. (A) HUVEC were used to assess uptake of CF660-labeled PEG–PLGA nanoparticles (CF660-NP, red). Lysosomes were stained by LysoTracker (green) dye, and cell nuclei were stained using DAPI (blue). Fluorescence confocal imaging of the HUVEC 1 h postincubation with CF660-NP showed significant uptake. CF660-NPs were detected inside HUVEC. (B) Histogram of FACS analysis showed a high count of CF660-NPs in HUVEC. (C) No differences were seen in HUVEC viability at 48 and 72 h incubation compared to control, as assessed by flow cytometry. (D) Mouse heart was perfused with IR800-labeled PEG–PLGA nanoparticle (IR800-NP) from inferior vena cava (IVC) and immersed in UW (University of Wisconsin) solution for 2 h at 4 °C. (E) Hearts perfused with IR800-NP were imaged by a UVP iBox Explorer imaging microscope, and a strong fluorescent signal was detected. (F) Hearts perfused with either phosphate-buffered saline (PBS) or IR800-NP were transplanted into recipient mice and harvested on the next day. The heart perfused with IR800-NP showed a strong fluorescent signal in contrast to the PBS-perfused heart. (G) Heart perfused with IR800-NP (red) was assessed histologically 1 day and 7 days post-transplant. Many IR800-NPs were detected between myocytes (F-actin, green) at day 1, and IR800-NPs were still detectable 7 days post-transplant. DAPI was used to stain cell nuclei (blue). (H) IR800-NPs were observed outside the vasculature (CD31, green) at day 1 post-transplant. (I) IR800-NPs were found inside the cytoplasm of CD11b⁺ cells and some CD11b⁻ cells at 1 day post-transplant. (J) At day 1 post-transplant, intra-allograft mean fluorescent intensity (MFI) of IR800-NP was significantly higher in CD11b⁺ cells compared to that in CD31 (control vs CD31 vs CD11b, 1.1 ± 0.01 vs 10.4 ± 0.5 vs 59.8 ± 2.6 , *** $p < 0.001$, $n = 3/\text{group}$).

affected organ is accessible for intraorgan delivery of therapeutics. Targeted delivery of nanoparticle-based therapeutics holds significant potential to improve treatment efficacy and reduce the off-target toxicity that plagues the clinical management of transplant recipients.

Mycophenolate mofetil (MMF) blocks inosine monophosphate dehydrogenase and inhibits purine metabolism in lymphocytes, preventing their proliferation. It is one of the most commonly used immunosuppressive agents following transplantation and has an excellent safety profile.²¹ We have

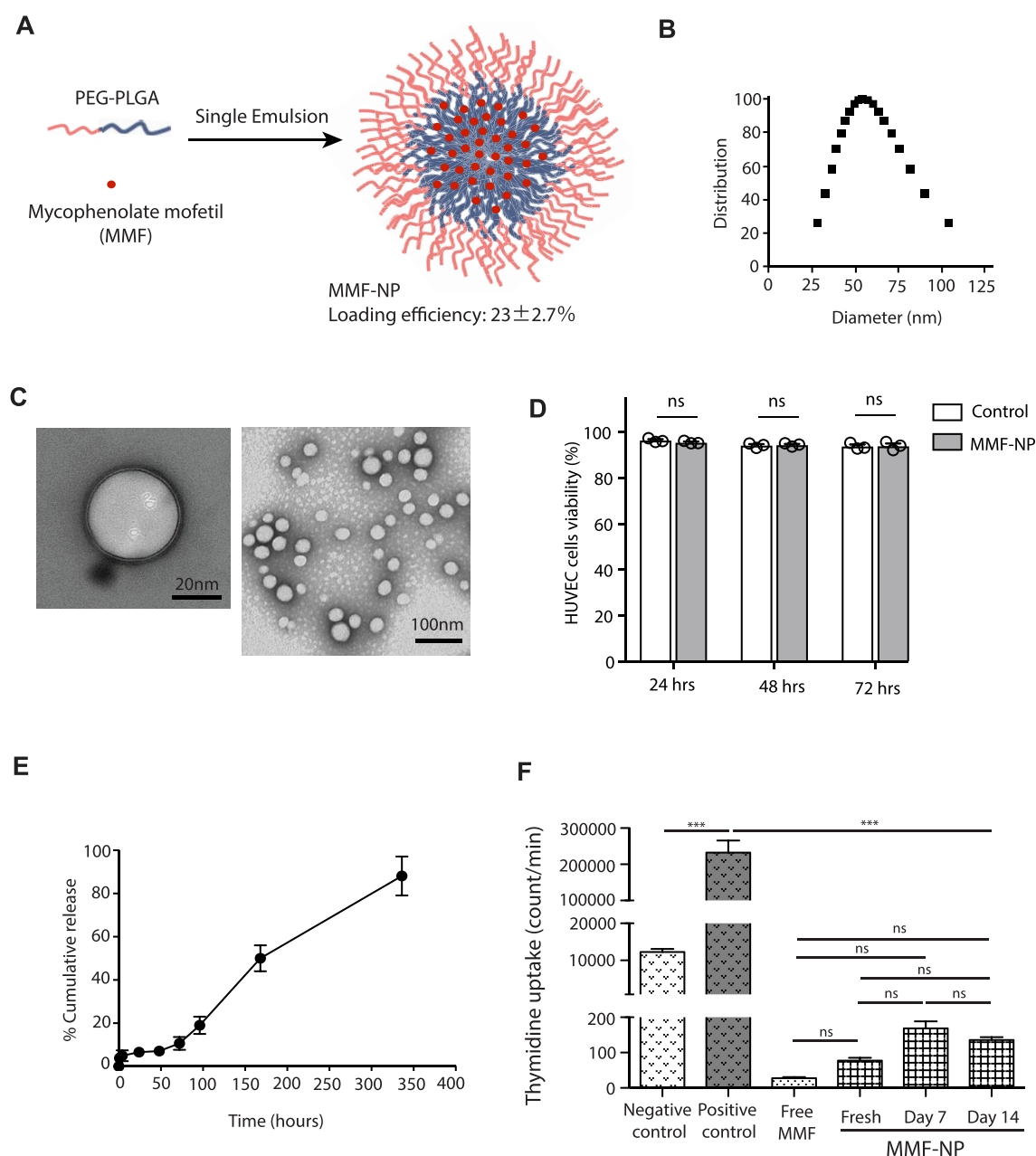


Figure 2. Synthesis and characterization of MMF-NP. (A) Schematic of MMF-NP fabrication. (B) Dynamic light scattering measurements of MMF-NP. (C) Transmission electron microscopy image of NPs (stained with 3% uranyl acetate). (D) HUVEC viability incubated with MMF-NP showed no difference in 24, 48, and 72 h compared to control. (E) *In vitro* release profile of MMF from NP. (F) T cell stimulation assay either with control, free MMF, or MMF-NP (freshly prepared, 7 days, and 14 days post-MMF release experiment). MMF-NP suppressed T cell proliferation, as measured by thymidine incorporation, with no differences between fresh, 7 days and 14 days post-MMF release.

engineered a nanoparticle carrier of MMF with excellent loading and release capacity. Herein, we tested the hypothesis that preperfusion of the donor heart with MMF-loaded PEG–PLGA nanoparticles (MMF-NPs) reduces early intragraft inflammation and prevents cardiac transplant vasculopathy and fibrosis.

RESULTS

Uptake of PLGA Nanoparticles by Human Umbilical Vein Endothelial Cells. To assess the effect of perfusion with PEG–PLGA NPs (size: 65 nm) on endothelial cells, we first measured their uptake by human umbilical vein endothelial cells (HUVEC) as a model of endothelium.^{22,23} PEG–PLGA nanoparticles labeled with CF660 dye (CF660-NPs, red

fluorescence) were incubated with HUVEC for 1 h. Lysosomes were stained using LysoTracker (green) dye, and images were taken by confocal microscopy. CF660-NPs were detected outside of lysosomes and located around the nuclei of HUVEC (Figure 1A). Intracellular CF660-NPs were counted by flow cytometry, which confirmed the uptake of CF660-NP by HUVEC within 1 h of incubation (Figure 1B). To assess if NPs had an effect on HUVEC viability, NPs were incubated with HUVEC for 48 and 72 h. FACS analysis of the cells showed that, even after 72 h of incubation, NPs did not cause any cell death (Figure 1C).

***In Vivo* Perfusion of Heart with PEG–PLGA Nanoparticles.** To study the kinetics of nanoparticles (NPs)

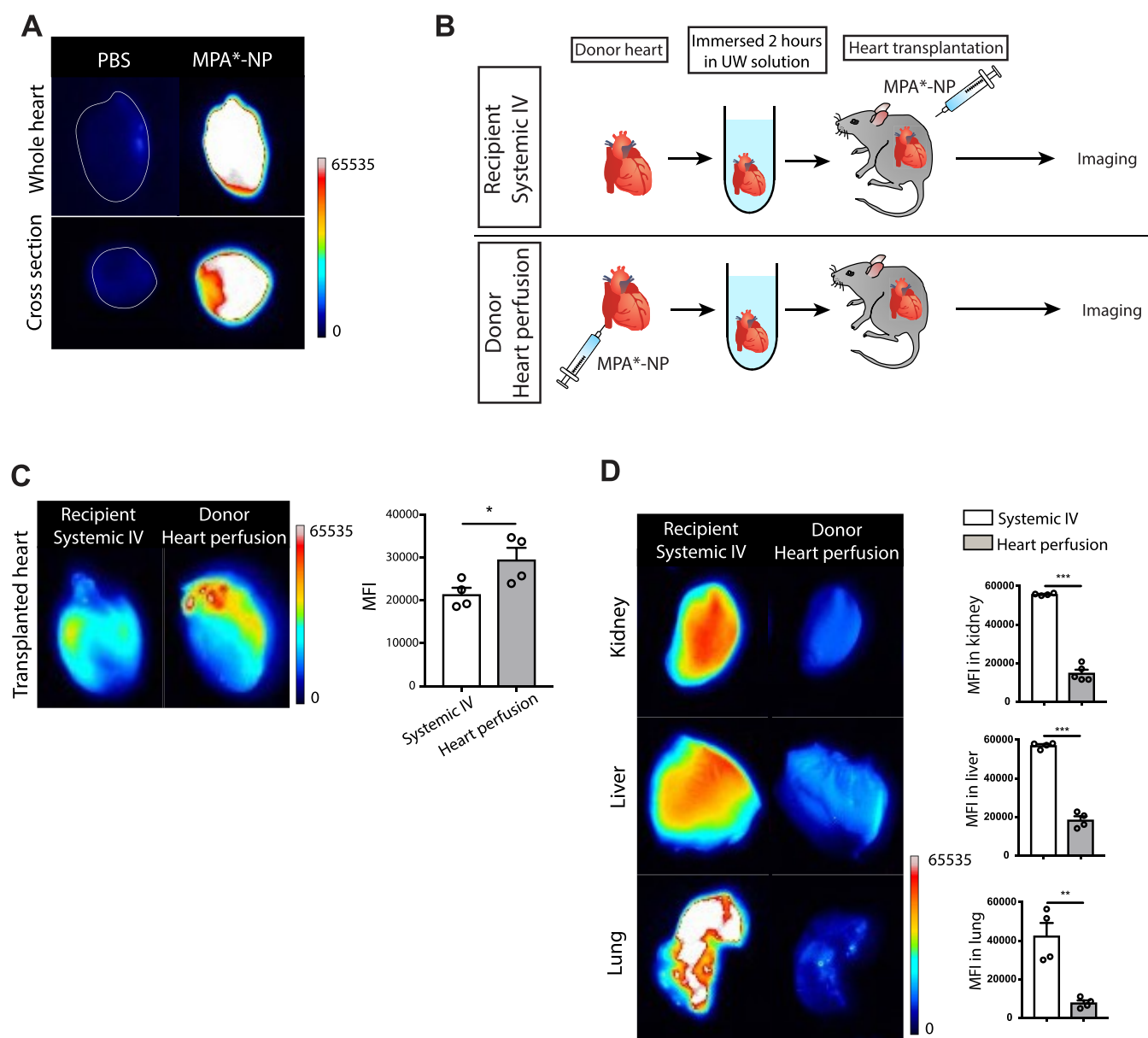


Figure 3. Biodistribution of MPA*-NP. (A) Heart perfused with MPA*-NPs showed high signal in the whole image and cross-sectional image compared to the heart perfused with PBS. (B) Schematic describes two group study designs. MPA*-NP was injected intravenously into recipient mice in the IV MPA*-NP group. MPA*-NP was perfused into the donor heart, and the perfused heart was transplanted into recipient mice in the MPA*-NP perfusion group. (C) Heart allograft in the MPA*-NP perfusion group showed a MPA*-NP signal significantly higher than that of the heart allograft in the IV MPA*-NP group (IV MPA*-NP group vs MPA*-NP perfusion group, 21401 ± 1560 vs 29526 ± 2742 , $*p < 0.05$, $n = 4$ mice/group). (D) Kidney, liver, and lung harvested from the MPA*-NP perfusion group showed a MPA*-NP signal significantly lower than that of the IV MPA*-NP group (IV MPA*-NP group vs MPA*-NP perfusion group, 55689 ± 289 vs 14806 ± 1810 , $***p < 0.001$ for kidney, 56995 ± 788 vs 18375 ± 1995 , $***p < 0.001$ for liver, 42411 ± 5743 vs 7712 ± 1330 , $**p < 0.01$ for lung, $n = 4$ mice/group).

following delivery to the heart, we synthesized PLGA NPs loaded with IR800 CW (IR800-NP). IR800 CW is a near-infrared (NIR) fluorophore.

Mice underwent thoracotomy, and the heart was perfused with IR800-NP *via* injection into the inferior vena cava. The heart was then harvested and immersed in UW (University of Wisconsin) solution at 4 °C for 2 h (Figure 1D), and it was imaged using an iBox Explorer2 imaging microscope (UVP). The fluorescent signal detected from the entire heart organ demonstrated uniform perfusion of heart tissue with IR800-NP (Figure 1E).

Next, to assess the trafficking of NP following transplantation, a heart perfused with IR800-NP as described above was

transplanted into C57BL/6 mouse.^{24,25} At day 1 post-transplantation, an IR800 fluorescent signal was detectable from the transplanted heart perfused with IR800-NP, as compared to a heart perfused with phosphate-buffered saline (PBS) (Figure 1F).

Mice were sacrificed at day 1 and day 7 postcardiac transplant, and immunofluorescence analysis of the allograft revealed the presence of IR800-NP (red) within the cardiac tissue (green, F-actin) at both time points (Figure 1G). We next examined the distribution of IR800-NPs in vascular and nonvascular compartments of the cardiac allograft. Co-staining with CD31 and CD11b demonstrated that the vast majority of IR800-NPs were located within CD11b⁺ cells (Figure 1H–J).

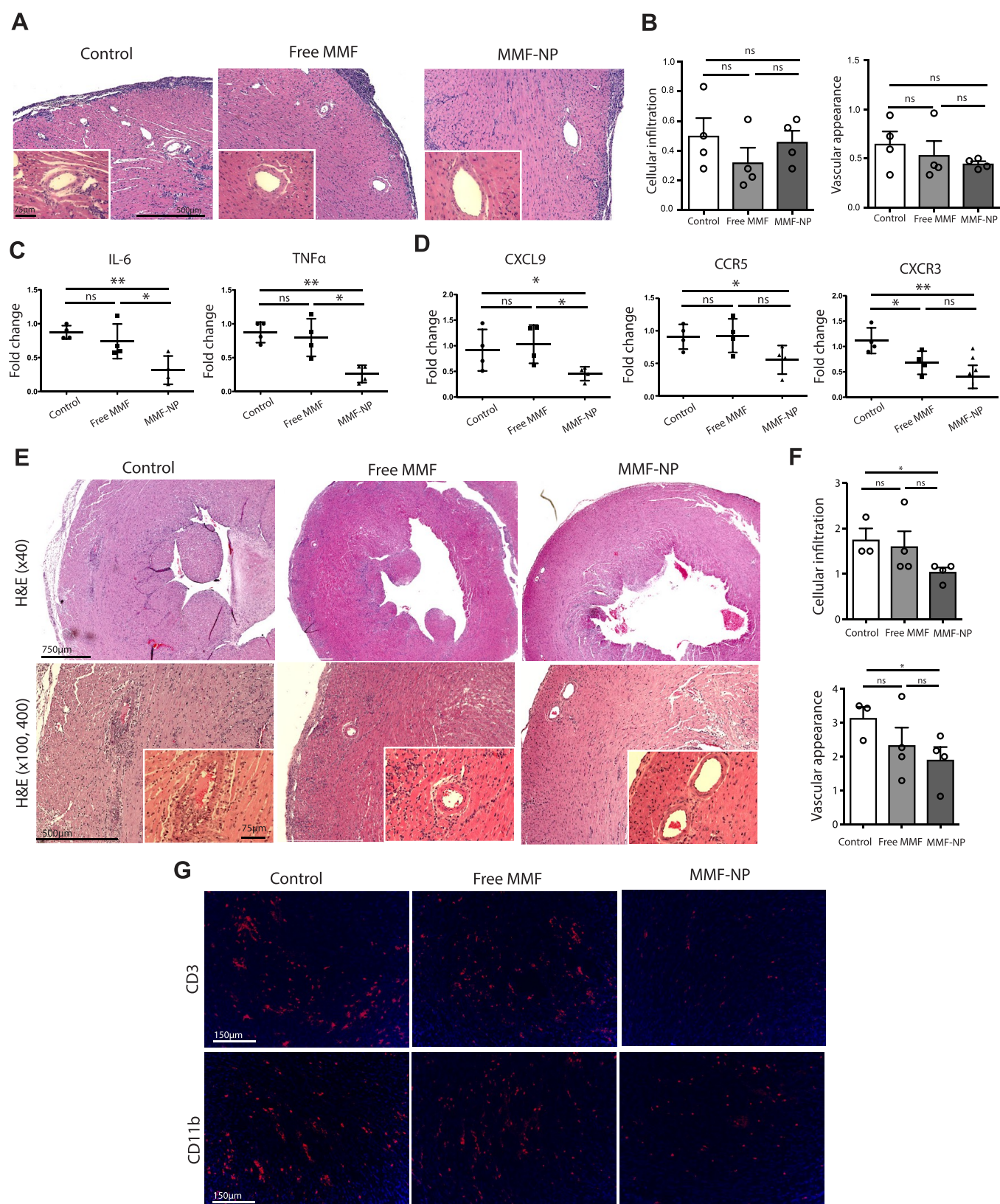


Figure 4. Early intragraft immune response suppression by MMF-NP. (A) H&E staining of the heart allografts perfused with PBS (control), free MMF, or MMF-NP 5 days post-transplantation. No difference in light microscopic evidence of rejection, including cellular infiltration or vascular injury, was detected in heart grafts among the three groups. (B) No difference of cellular infiltration and vascular appearance score was found among the three groups (control vs free MMF vs MMF-NP, 0.50 ± 0.12 vs 0.32 ± 0.61 vs 0.45 ± 0.07 for cellular infiltration, 0.65 ± 0.13 vs 0.53 ± 0.14 vs 0.45 ± 0.02 for vascular appearance score, $n = 4$ mice/group). (C) Analysis of heart allografts by qPCR showed significantly lower expression of IL-6 and TNF α in the heart grafts perfused with MMF-NP compared to the control and free MMF groups (control vs free MMF vs MMF-NP, 0.87 ± 0.05 vs 0.74 ± 0.13 vs 0.31 ± 0.10 for IL-6, 0.87 ± 0.07 vs 0.79 ± 0.14 vs 0.25 ± 0.06 for TNF α , $n = 4$ mice/group).

Figure 4. continued

(D) Expression of CXCL9 was reduced significantly in the heart allograft perfused with MMF-NP, as compared to the control and free MMF groups (control vs free MMF vs MMF-NP, 0.91 ± 0.20 vs 1.03 ± 0.18 vs 0.45 ± 0.06 for CXCL9, $n = 4$ mice/group). A trend toward reduction was also observed for the expression of CCR5 and CXCR3 in the MMF-NP group (control vs free MMF vs MMF-NP, 0.91 ± 0.09 vs 0.92 ± 0.12 vs 0.55 ± 0.10 for CCR5, 1.11 ± 0.12 vs 0.68 ± 0.11 vs 0.40 ± 0.11 for CXCR3, $n = 4$ mice/group). (E) H&E staining of the heart allografts at 14 days post-transplant. Control heart showed moderate cellular infiltration of the myocytes and vasculopathy. Mild cellular infiltration of the myocytes and clear vasculature were observed in free MMF group. The heart graft perfused with MMF-NP had scant cellular infiltration of myocytes and clear vasculature. (F) Heart allograft perfused with MMF-NP showed significantly lower cellular infiltration and vascular appearance compared to that with the control group (control vs free MMF vs MMF-NP, 1.67 ± 0.33 vs 1.41 ± 0.34 vs 0.48 ± 0.13 for cellular infiltration, 2.52 ± 0.74 vs 1.31 ± 0.19 vs 0.72 ± 0.13 for vascular appearance score, $n = 3-4$ mice/group). (G) Very few CD3⁺ T cells and CD11b⁺ cells infiltrates were observed in the heart allograft perfused with MMF-NP, as compared to that with the control and free MMF groups.

Synthesis and Characterization of MMF-Loaded PEG-PLGA NP (MMF-NP). Mycophenolate mofetil (MMF; Cellcept) is a prodrug of mycophenolic acid (MPA), an inhibitor of inosine monophosphate dehydrogenase (IMPDH). It is routinely used systemically for prevention of rejection in kidney, liver, and heart transplantation.^{21,26-28} We chose MMF to target the organ for pretreatment, due to its excellent vascular safety profile and lack of end-organ toxicity.^{29,30} A mix of polymer and MMF in ethyl acetate was emulsified in the water phase, followed by solvent evaporation and MMF-loaded PEG-PLGA NP (MMF-NP) collection by centrifugation (Figure 2A). The loading efficiency of MMF was calculated as $23 \pm 2.7\%$, which is equivalent to $39 \mu\text{g}$ of MMF per dose. The average size of our MMF-NP was around 60 nm (Figure 2B), and it was negatively charged (-16.2 ± 0.67) by dynamic light scattering (DLS) measurement. Observation under electron microscopy highlighted its round shape, double layer, and size (Figure 2C).

Kinetics of MMF Release from MMF-NP *in Vitro*. First, we tested for toxicity of MMF-NPs on HUVEC. MMF-NPs were incubated with HUVEC for 24, 48, and 72 h. We did not observe any toxic effects of MMF-NPs on HUVEC (Figure 2D). Next, the release profile of MMF from MMF-NPs was measured *in vitro* under physiological conditions. MMF was released gradually from the NPs during the first 3 days of release, achieved 60% release by day 7, and the release kinetics remained controlled through day 10 (Figure 2E).

We then examined the retaining and releasing capacity of MMF from MMF-NPs by testing its ability to suppress T cell proliferation *in vitro*. We compared MMF-NPs to the same amount of free MMF ($39 \mu\text{g}$). MMF-NPs and free MMF suppressed T cell proliferation equally (Figure 2F). To assess the clinical applicability of this approach, we were also interested in examining the retention of MMF and testing its immunosuppressive capacity following long storage. MMF-NPs, which were stored for 7 and 14 days, were washed thoroughly and added to a T cell suppression assay. MMF-NPs from both time points showed effective suppression of T cells (Figure 2F), demonstrating the stability of these NP over time.

Biodistribution of Labeled MPA Following Intraorgan Perfusion. To observe the distribution of our NP *in vivo*, we used a labeled form of MPA to generate fluorescent NPs. For these experiments, we utilized MPA, instead of its pro-drug MMF, as MPA can be conjugated easily with amine-containing dyes to enable tracking *in vivo*. We labeled MPA directly with an amine-functionalized fluorescent dye (amine CF594) (MPA*) and synthesized NPs (MPA*-NPs).

To assess our ability to detect MPA*-NPs in tissue, hearts were perfused either with PBS or MPA*-NPs, harvested, and immersed in UW solution for 2 h. The heart perfused with

MPA*-NPs showed a strong fluorescent signal in both whole heart and cross-sectional images, as compared to the PBS group (Figure 3A).

Next, we wanted to assess the degree of accumulation of MPA* in the heart allograft when the donor allograft is perfused with MPA*-NP prior to transplant (MPA*-NP perfused group), as compared to transplanting the recipient with a nonperfused heart, and then treating the recipient with systemic intravenous MPA*-NP at the time of transplantation (IV MPA*-NP group) (Figure 3B). Six hours after heart transplantation, organs from transplanted animals were harvested for bioluminescence study to assess the biodistribution of MPA*-NP. Transplanted hearts from the MPA*-NP perfused group showed a fluorescent signal significantly higher than that of the heart grafts from the IV MPA*-NP group (Figure 3C). Other organs, such as kidney, liver, and lung, revealed greater accumulation of MPA*-NP and a MFI in recipients from the IV MPA*-NP group significantly higher than that of the MPA*-NP perfused group (Figure 3D). These data indicate that MPA was delivered to the donor heart effectively with perfusion prior to organ transplantation and remained localized, without accumulation in other organs.

Suppression of Early Intraorgan Alloimmune Response by MMF-NP. Our next objective was to examine the *in vivo* efficacy of MMF-NP in a MHC class II mismatch mouse heart transplant model of chronic allograft rejection. A BM12 mouse heart (donor heart) was perfused with either PBS (control), free MMF, or MMF-NP, harvested, and immersed in UW solution at 4 °C. Two hours later, the heart was transplanted into a C57BL/6 mouse (recipient).

Based on the findings from our previous experiment evaluating the tempo of MMF release from the NP (refer Figure 2E), we harvested heart allografts at day 5 post-transplantation. As expected in this model of chronic allograft rejection, no difference in cellular infiltration or vascular appearance of the heart grafts between the groups on day 5 was observed, as assessed by scoring of H&E images the modified ISHLT score (Figure 4A,B). However, analysis of heart allografts by qRT-PCR revealed that the allografts perfused with MMF-NP had significantly lower expression of pro-inflammatory cytokines, such as IL-6 and TNF α , in comparison to that of control and free MMF-treated grafts (Figure 4C). Heart allografts perfused with MMF-NP also demonstrated lower expression of other pro-inflammatory cytokines, such as IFN γ , IL-17, and IL-2, but these differences did not reach significance (data not shown). In addition, intraorgan expression of chemokines was also assessed by qRT-PCR. Significant reductions in the expression of CXCL9 was observed in the heart allografts perfused with MMF-NP, as compared to control and free MMF (Figure 4D). Treatment with both MMF-NP and free MMF also led to a significant decrease in expression of

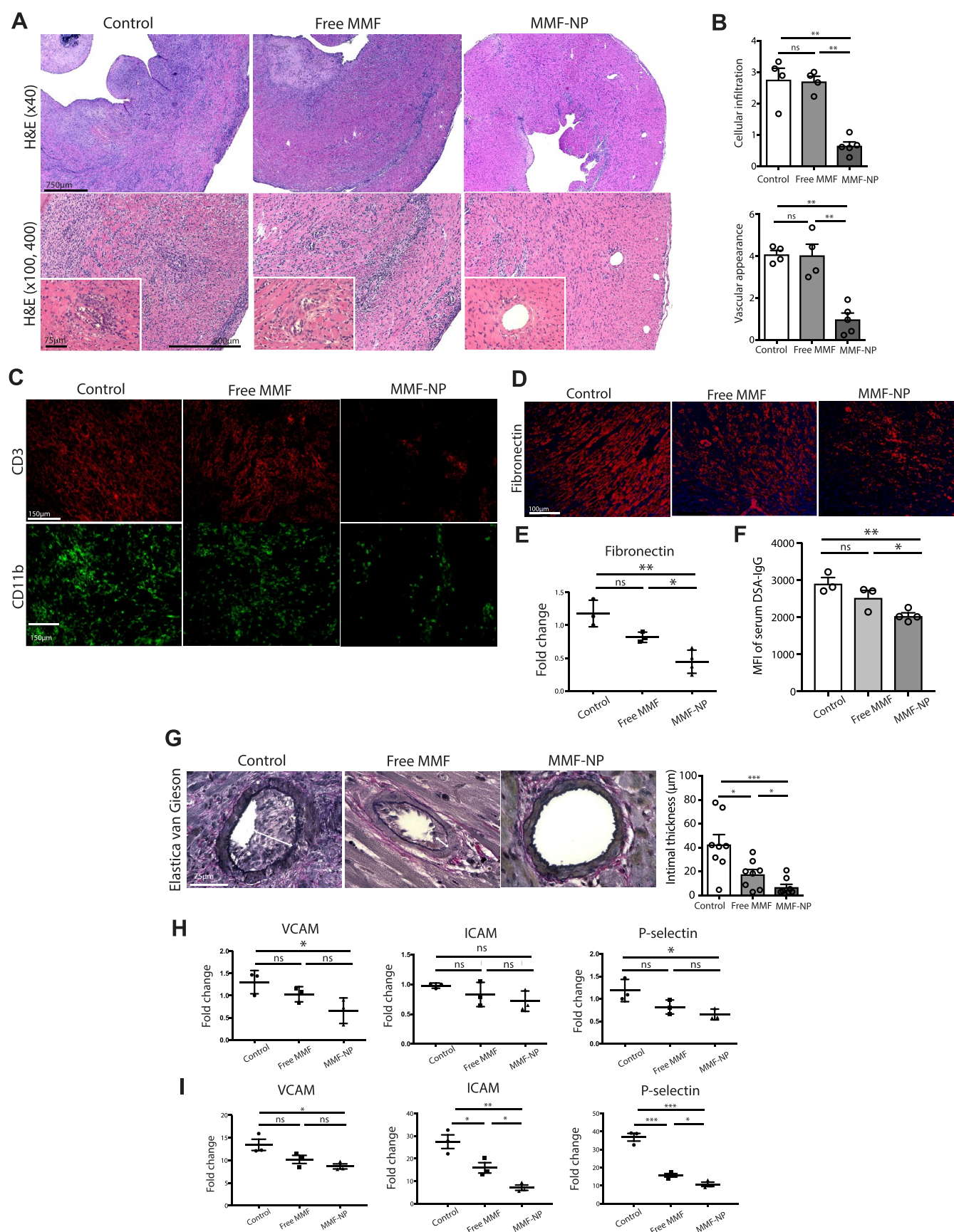


Figure 5. Perfusion of donor heart with MMF-NP prior to transplant showed marked effect within the graft and abrogated chronic allograft vasculopathy. (A) H&E staining of the heart allografts at 28 days post-transplant. Control heart contained moderate to severe cellular infiltration and occluded vasculature. The heart graft perfused with free MMF contained moderate cellular infiltration and vasculopathy. The heart graft perfused with MMF-NP contained much lower cellular infiltration and intact vasculature. (B) Histological scoring of both cellular

Figure 5. continued

infiltration and vascular appearance showed significantly lower scores in the MMF-NP group, as compared to the control and free MMF group (control vs free MMF vs MMF-NP, 2.67 ± 0.30 vs 2.69 ± 0.17 vs 0.91 ± 0.28 for cellular infiltration, 4.01 ± 0.19 vs 4.03 ± 0.54 vs 1.43 ± 0.52 for vascular appearance score, $n = 4$ mice/group). (C) Very low infiltration of CD3⁺ and CD11b⁺ cells was observed in the heart allograft perfused with MMF-NP in comparison to control and free MMF groups. (D) Fibronectin staining showed lower fibrosis in MMF-NP group compared to control and free MMF groups. (E) Gene expression of fibronectin showed significantly lower expression in the allograft heart harvested from MMF-NP group compared to control and free MMF groups (control vs free MMF vs MMF-NP, 1.2 ± 0.12 vs 0.8 ± 0.04 vs 0.4 ± 0.08 , $n = 3$ mice/group). (F) MFI of DSA-IgG in serum from 28 days post-transplant in the MMF-NP group was significantly less than that in the control and free MMF groups (control vs free MMF vs MMF-NP, 2914 ± 156 vs 2532 ± 194 vs 2043 ± 79 , $n = 4$ mice/group). (G) Elastica van Gieson stain of the allograft heart showed thinner intima in the MMF-NP group compared to that in the control and free MMF groups (control vs free MMF vs MMF-NP, 42.6 ± 8.4 vs 17.6 ± 4.1 vs 6.8 ± 2.4 , 2 random arteries from each mouse, $n = 4$ mice/group). (H) Gene expression of VCAM, ICAM, and P-selectin in the allograft heart showed significantly lower expression in MMF-NP group compared to control (control vs free MMF vs MMF-NP, 1.3 ± 0.1 vs 1.0 ± 0.1 vs 0.6 ± 0.1 for VCAM, 0.9 ± 0.02 vs 0.8 ± 0.1 vs 0.7 ± 0.09 for ICAM, 1.2 ± 0.1 vs 0.8 ± 0.08 vs 0.6 ± 0.06 for P-selectin, $n = 3$ mice/group). (I) HUVEC stimulated by TNF α showed high expression of VCAM, ICAM and P-selectin, which were suppressed by adding MMF-NP to a greater degree than by free MMF (control vs free MMF vs MMF-NP, 13.4 ± 1.2 vs 10.2 ± 0.9 vs 8.6 ± 0.5 for VCAM, 27.4 ± 3.0 vs 15.9 ± 2.3 vs 7.1 ± 1.2 for ICAM, 36.8 ± 2.1 vs 15.7 ± 0.9 vs 10.7 ± 1.2 for P-selectin, $n = 3$ mice/group).

CCR5 and CXCR3 as compared to expression of the control, although no difference was seen between the two MMF formulations (Figure 4D).

On the basis of our findings that MMF-NP suppresses T cell proliferation up to 14 days *in vitro*, we next assessed the status of heart grafts at 14 days post-transplantation. Heart allografts in all three groups (control, free MMF, and MMF-NP) were beating at 14 days post-transplant when they were harvested for analysis. Histologic assessment revealed moderate cellular infiltration and vasculopathy in the control group, whereas those perfused with free MMF had mild cellular infiltration and clear vasculature (Figure 4E). Furthermore, heart grafts in the MMF-NP group had little cellular infiltration of the myocytes and clear vasculature (Figure 4E). Consequently, grafts perfused with MMF-NP showed scores for cellular infiltration and vascular pathology significantly lower than those of the control, but these differences did not reach statistical significance in comparison with the free MMF group (Figure 4F). Immunofluorescent staining revealed fewer CD3⁺ T cells and CD11b⁺ cells in heart allografts perfused with MMF-NP, as compared to control and free MMF-perfused hearts (Figure 4G).

Pretransplant Donor Heart Perfusion with MMF-NP Abrogates Cardiac Transplant Vasculopathy. Using this MHC class II mismatch model of chronic rejection, we next performed longer-term observation of the allografts to assess the effect of MMF-NP perfusion at the time of allograft retrieval. At 28 days post-transplant, we harvested the heart allografts, spleens, and draining lymph nodes (DLNs) of recipient mice whose grafts were perfused with either PBS (control), free MMF, or MMF-NP prior to transplantation. All heart allografts were beating at 28 days post-transplant, but the strength of contraction of hearts in the control and free MMF groups were weaker than that in the MMF-NP-treated group. Histologic analysis of the heart allografts in the control group revealed moderate to severe cellular infiltration and occluded vasculature (Figure 5A). In comparison to their appearance at 14 days post-transplantation (refer to Figure 4E, free MMF), by day 28, the heart allografts perfused with free MMF showed progressive graft injury with moderate cellular infiltration and vasculopathy (Figure 5A). In comparison, allografts perfused with MMF-NP showed much lower cellular infiltration and intact vasculature, consistent with less severe injury (Figure 5A), and their histological appearances were similar to those harvested at day 14 (refer to Figure 4E, MMF-NP). We observed significantly lower scores for both cellular infiltration and vascular appearance in the MMF-NP group in comparison to the control

and free MMF groups (Figure 5B), which supported the observations of H&E-stained tissue. The immunofluorescence staining of heart allografts also contained lower infiltration of CD3⁺ T cells and CD11b⁺ cells in the MMF-NP group, as compared to the control and free MMF groups (Figure 5C).

Interstitial fibrosis is an important feature of chronic allograft injury.^{31,32} The heart allografts treated with MMF-NP contained significantly less fibronectin staining, as compared to that of the control and free MMF groups (Figure 5D). Furthermore, the gene expression of fibronectin in allograft hearts was significantly lower in the MMF-NP group (Figure 5E). We also measured the development of donor-specific antibody (DSA) to assess the chronic alloimmune response. Serum samples collected at day 28 post-transplant were analyzed by FACS to detect DSA-IgG. As shown in Figure 5F, serum collected from the MMF-NP group demonstrates DSA-IgG development significantly lower than that of other groups. We also evaluated chronic allograft vasculopathy (CAV).³³ Elastica van Gieson stain of heart allografts harvested on day 28 showed a significant increase of intimal thickness in control and free MMF-treated recipients (white arrows). However, the vasculature in those treated with MMF-NP showed less intimal thickening (Figure 5G).

The expression of VCAM, ICAM, and P-selectin on endothelium has also been used to assess vasculopathy.^{33,34} We next assessed the expression of these genes in allograft hearts and observed a significant suppression of VCAM and P-selectin expression in the MMF-NP group as compared to that of the control (Figure 5H). To examine the effect of MMF-NP on endothelial cells in greater detail, we also assessed the level of VCAM, ICAM, and P-selectin gene expression *in vitro*, using HUVEC stimulated with TNF α and incubated with either free MMF or MMF-NP. Whereas the expression of these genes was very low in untreated HUVEC, we noted a marked increase following stimulation with TNF α . This increase was markedly and significantly suppressed by MMF-NP treatment, as compared to that of the control group, and additional suppression was seen in comparison to treatment with free MMF alone (Figure 5I).

Lack of Systemic Effect of Allograft Preperfusion with MMF-NP Despite Prolonged Local Effect on Heart Allograft. Given the superior histological appearance of the allograft at 28 days post-transplant, we were interested to assess if graft perfusion with MMF-NP prior to transplantation had an effect on peripheral immune responses. Spleens and DLNs harvested on day 28 post-transplant from mice treated with MMF-NP, free MMF, and control (PBS) were analyzed by flow

cytometry. We observed no differences in the percentages of CD4⁺ and CD8⁺ T cells in spleens or DLN between the three groups (Supplementary Figure S1A). Similarly, percentages of CD4⁺CD62L^{low}, CD8⁺CD62L^{low}, CD4⁺CD69⁺, CD8⁺CD69⁺, and CD4⁺CD25⁺Foxp3⁺T cells in the spleen and DLN were not statistically different among the three groups (Supplementary Figure S1B).

We then tested the effect of intraorgan delivery on the peripheral alloimmune responses using Elispot and mixed lymphocyte reaction (MLR) of spleen and DLN. In Elispot analysis, we observed no statistically significant differences between groups in spleen and DLN (Supplementary Figure S1C). MLR assay also showed no statistically significant differences between groups in cells harvested from the spleen or DLN (Supplementary Figure S1D). These findings suggested that the selective perfusion of heart allografts with MMF-NP suppressed the local intraorgan alloimmune response, but it did not affect the systemic immune response.

DISCUSSION

The majority of transplanted organs undergo hypothermic perfusion between procurement and transplantation, which provides the opportunity to add therapeutic agents, including nanocarriers, into the preservation fluid. Direct delivery of ISAs to the organ at the time of transplantation could potentiate their efficacy by decreasing intraorgan inflammation and alloimmune activation during this critical period. This approach could also potentially decrease the need for systemic exposure to ISAs, such as calcineurin inhibitors, which have been implicated in microvascular toxicity, accelerated cardiovascular disease, and malignancies.^{1,35–40}

Allograft ischemia, which is unavoidable in transplantation, is one of the most significant stimuli of intraorgan inflammation. Several noteworthy studies have emphasized the importance of intraorgan immune activation in orchestrating allograft rejection.^{41–43} Intraorgan inflammatory responses can lead to increased alloimmunity *via* activation of resident dendritic cells.^{12,13,44–50} Early innate inflammatory responses have been found to be regulated critically by IFN γ -producing endogenous CD8⁺ T cells present in the recipient before detectable priming of alloantigen T cells.^{51,52} We have recently reported that early ischemic injury to the organ leads to increased intraorgan IL-6 production, thereby enhancing alloimmunity. Furthermore, perfusing organs with nanocarriers of anti-IL-6 prior to transplantation significantly improved transplant outcomes in a murine model of cardiac transplantation.¹²

T cells can be directly primed and stimulated by activated endothelial cells expressing adhesion molecules, along with class I and II MHC molecules.^{50,53–60} Furthermore, endothelial cells may also play a role in recruiting recipient antigen-presenting cells (APC) to the organ,^{61–64} indicating their central role in orchestrating early alloimmune responses. Recognizing the therapeutic potential of targeted intraorgan drug delivery in transplantation, several other groups have also applied nanotechnology to deliver therapeutics to the endothelium in organs for transplant. *Ex vivo* machine perfusion has been used to deliver therapeutics to human kidneys and blood vessels prior to transplant and led to a reduction in intraorgan activated T cells.^{22,23,65} These studies together emphasize the impact of the intraorgan immune response in the pathogenesis of graft rejection and highlight the importance of engineering therapies aimed at disrupting its development.

In clinical practice, MMF and MPA are routinely and interchangeably used in organ transplantation, due to both efficacy and vascular and metabolic safety profile.^{21,66} We chose MMF for our NP for delivery to the heart allograft, as it has lower polarity than MPA because of the masking of polar carboxylic groups, which leads to higher loading efficiency in emulsification as well as slower release kinetics from the NP that thereby generate a more effective therapeutic product. MMF, a prodrug of MPA, inhibits inosine monophosphate dehydrogenase (IMPDH), interfering with purine synthesis and proliferation of lymphocytes.^{67–69} MMF also blocks glycosylation of lymphocyte and monocyte glycoproteins required for adhesion to endothelial cells and inhibits leukocyte recruitment into areas of inflammation by reducing the expression of adhesion molecules such as E- and P-selectin.^{70,71} Therefore, early application of MMF to harvested organs could target alloimmune responses on multiple levels.⁷² Similar to previous reports,^{22,23,73} we first assessed the uptake and toxicity of our PEG–PLGA NP by HUVEC. In keeping with our findings with other NPs, these studies indicated that MMF-NP had no toxic effect on HUVEC. We examined the kinetics of release of MMF, which showed a sustained release pattern, and we demonstrated the stability of these NP, as both freshly manufactured and stored MMF-NP suppressed T cell proliferation effectively *in vitro*. These data suggest that perfusion of organs prior to transplant not only suppresses immediate events in alloimmune activation, but it also could dampen the later phases of chronic rejection, as well.

We targeted the donor organ through direct perfusion with IR800-NP prior to transplantation, and we assessed the distribution of IR800-NP within the organ pre- and post-transplantation. The perfused heart contained a strong signal prior to transplantation, and NPs could be distinguished clearly following transplantation, located between the F-actin filaments of the perfused heart. Perfused NPs were taken up mainly by CD11b⁺ cells, such as macrophages or monocytes. Therefore, targeted therapies aimed specifically toward macrophages could be achieved potentially using this approach.

One important issue was to assess the superiority of NPs in delivering drug to the allograft while avoiding peripheral tissue accumulation. To answer this question, we generated NPs with labeled drug and examined the resulting *in vivo* signal to observe their distribution. For these labeling experiments, we selected MPA over MMF due to technical considerations. Unlike MMF, MPA has a carboxylic acid, which can be conjugated easily with amine-containing dyes by carboxylamine cross-linking *via* carbodiimide-mediated coupling chemistry. MPA labeled with amine CF594 (MPA*) was placed inside a NP (MPA*-NP) and perfused to the heart allograft prior to transplant, and we examined the distribution of its signal *in vivo* in comparison to systemic IV administration into recipient mice. As expected, MPA*-NP-perfused cardiac allografts contained a MPA*-NP signal higher than that of cardiac allografts exposed only to MPA*-NP *via* intravenous injection into the recipient, whereas the other major organs showed a lower signal in the recipients of MPA*-NP-perfused hearts. These results clarified the effectiveness of our selective drug delivery and emphasized the advantages of this perfusion strategy with respect to avoidance of off-target effects on other vital organs.

Then, we used a model of chronic allograft rejection, an MHC class II mismatch murine heart transplant model, to test the efficacy of MMF-NP in impacting this process at several time points. This model does not replicate all features of chronic

rejection observed in humans but demonstrates early features of vascular injury. Reflecting the insidious development of vascular allograft injury, cellular infiltrates or vascular injuries were not prominent at day 5 post-transplantation in any of the treatment groups. Nonetheless, we examined the mRNA transcripts of inflammatory cytokines as more sensitive markers of early inflammatory responses. Significant reductions in IL-6, TNF α , and IFN γ were observed, along with reductions in key pro-inflammatory chemokines.^{74–80} MMF inhibits T lymphocyte proliferation directly through its classical mechanism of action and is also known to decrease expression of adhesion molecules by endothelial cells.^{70,71} The effect of MMF on endothelial cells is independent of its effect on nucleotide synthesis.⁸¹ MMF blocks TNF α induced expression of adhesion molecules by endothelial cells *via* effects on intracellular signaling pathways, namely, inhibition of phosphorylation of MAP kinases, decreased in reactive oxygen species generation, and inhibition of nuclear translocation of NF- κ B p65.⁸²

Our mechanistic data support a role for MMF in decreasing local inflammation within the graft at the time of transplant, and these findings suggest that decreased lymphocyte trafficking into the transplant may be an important mechanism for the observed improved allograft outcomes.

By day 28 post-transplantation, both the control group and free MMF groups had much more severe allograft damage than did the MMF-NP-treated grafts. Immune characterization of T cells and macrophages also showed a marked reduction in these cells.

The major characteristics of chronic allograft rejection are fibrosis and allograft vasculopathy.^{31–33,83} Although the mouse model cannot replicate all features of chronic allograft rejection in humans, in cardiac allografts harvested at 28 days following transplantation, we observed significantly less fibrosis, lower expression of VCAM and P-selectin, and lesser degrees of intimal thickening in the MMF-NP-treated recipients. To more directly examine the effect of MMF-NP on endothelial cell activation, we also returned to the *in vitro* model of TNF α stimulated HUVEC, incubated either with PBS, free MMF, or MMF-NP, and we found a significant reduction in the expression of adhesion molecules after incubation with MMF-NP, similar to our results in the heart allograft.

Examining the alloimmune responses in the lymphoid tissues of the host revealed no difference between groups, indicating that the impact of MMF-NP on allograft injury may be mediated solely by its effect on intragraft immune activation. Interestingly, we found lower levels of DSA in MMF-NP treated recipients, which suggests this treatment may have influenced antibody generation in the draining LN in addition to its local effects.

Great interest exists currently in the *ex vivo* perfusion of donor organs as a strategy to optimize grafts prior to transplantation.^{23,84–86} The method of static simple cold storage (SCS) is approved for liver grafts, whereas both SCS and dynamic hypothermic machine perfusion are clinically approved for kidneys. The potential to use ISA-loaded nanocarriers (ISA-NP) for targeted drug delivery has begun to attract considerable attention in the field of transplantation.^{12,23,24,87,88} Based on the model described here, we speculate that perfusing organs with ISA-NP using currently available perfusion machines could be a readily translatable strategy that could reduce early intragraft inflammation significantly, decrease alloimmune activation, and potentially improve longer-term outcomes. Such findings are supported by previous publications from others.^{88,89} By perfusing the donor graft with NPs loaded with agents to

oppose the pro-inflammatory effects of ischemia prior to transplantation, the disadvantage of prolonged ischemic time to transplant outcomes could also be mitigated.

An interesting future direction will be to investigate the optimal duration of perfusion with NP to maximize ISA delivery to the transplant organ. Devising a maximally effective strategy to apply this approach will require further evaluation.

Our strategy allows for the delivery of a wide range of combinatorial therapeutics other than ISAs, including drugs ranging from small molecules to antibodies, which underlines its vast potential therapeutic implications. Given the substantial clinical unmet needs in transplantation, we believe that intraorgan delivery of nanotherapeutics prior to transplantation could lead to substantial improvements in transplantation outcomes. The FDA has approved the biocompatible and biodegradable PEG–PLGA polymer used in this study for clinical applications, and its routine use in medical materials such as surgical sutures^{90–94} demonstrates its excellent safety profile.

CONCLUSIONS

In summary, our current study establishes a method of a controlled, gradual release of MMF through perfusion of the allograft, at the time of harvest with MMF-NP. Our data indicates that perfusion of heart allografts with MMF-NP prior to transplantation suppresses the early intragraft immune response and leads to decreased evidence of transplant vasculopathy and fibrosis post-transplantation.

METHODS

NP Incubation with HUVEC. HUVEC were plated in 4-well chambered Nunc Lab-Tek II chamber slides overnight. Then, CF660-NP suspensions were added to different wells and incubated for 1 h in a humidified 37 °C, 5% CO₂ incubator. The cells were washed with PBS three times and stained with DAPI and LysoTracker (LysoTracker Green DND-26).

HUVEC Viability Assessment. HUVEC were cultured in 6-well plates overnight (0.5×10^6 cells/mL). Empty NPs or MMF-NPs were added to the HUVEC at concentrations similar to what was used *in vivo*. The samples were incubated in a humidified 37 °C, 5% CO₂ incubator in triplicates for 24, 48, and 72 h. Cells cultured without any additional reagent were considered as control. Cells were washed three times with PBS at the end of incubation time, and dead cells were stained using eBioscience fixable viability dye eFluor 450 (cat# 65-0863-14). The cell suspension was analyzed using a FACS Canto II (BD Bioscience, Franklin Lakes, NJ) instrument.

Preparation and Characterization of MMF-NPs. We have engineered MMF-NPs using a single emulsion and solvent evaporation method. Briefly, poly(D,L-lactic-co-glycolic) acid copolymer (PLGA) was dissolved in ethyl acetate and mixed with MMF (in acetone). The mix was then emulsified in 3 mL of deionized water using probe sonication and homogenization over ice. The emulsion was added dropwise to 20 mL of deionized water and stirred for 2 h to evaporate the organic solvent. After solvent evaporation, the MMF-NP was collected and washed by centrifugation using Amicon Ultra-15 centrifugal filter units (MWCO 100 kDa) at 3000g for 30 min. The size and zeta-potential of MMF-NPs were assessed and characterized using DLS. The morphology of MMF-NPs was studied using scanning electron microscopy and transmission electron microscopy. The filtrate of the MMF-NP wash steps were collected, and the absorbances were then analyzed at 300 nm using a UV/vis spectrophotometer. The amount of MMF in the filtrate was quantified by comparing the absorbance at 300 nm with a calibration curve of various concentrations of MMF.

The loading efficiency was calculated as follows:

$$\text{loading efficiency (\%)} = (\text{MMFi} - \text{MMFf})/\text{MMFi}$$

where MMFi is the initial amount of MMF used to prepare MMF-NP and MMFf is the free nonloaded MMF determined in the last step.

Release Profile of MMF from MMF-NP. To quantify the release profile of MMF from NPs, the MMF-NP solutions were incubated in triplicates at 37 °C and assessed at defined time intervals (1, 2, and 4 h; 1, 2, 3, 4, 7, and 14 days). The samples were centrifuged at each time point using Amicon Ultra-15 centrifugal filter units (MWCO 10 kDa; Sigma-Aldrich) at 3000g for 15 min. The absorbances of the filtrate and MMF-NP suspension were then analyzed at 300 nm using a UV/vis spectrophotometer. The amount of released MMF at each time point was quantified by comparing the absorbance at 300 nm with a calibration curve of various concentrations of MMF.

T Cell Proliferation Assay. Splenocytes were isolated from the spleens of C57BL/6 mice and seeded at one million cells per well in a round-bottom 96-well plate. Next, cells were stimulated using anti-mouse CD3/CD28 antibodies (3 µg/mL in complete RPMI media). Free MMF and MMF-NP (freshly prepared, and 7 and 14 days post-MMF release experiment) were added to the cells. Unstimulated splenocytes were used as the negative control, and splenocytes stimulated with anti-mouse CD3/CD28 without the addition of MMF or MMF-NP were used as the positive control. The plate was placed in a humidified 37 °C, 5% CO₂ incubator for 2 days. Next, tritiated thymidine (³H) was added to each well, and the plate was returned to the incubator for 14 h. Cells were harvested using a semiautomated sample harvester and analyzed using a β scintillation counter.

Labeling of Mycophenolic Acid. MPA (10 mM) was prepared in a 4 mL vial dried under high vacuum for 24 h and dissolved in 100 µL of dimethylformamide (DMF) with (1*H*-benzotriazol-1-yl)-1,1,3,3-tetramethyluronium hexafluorophosphate (HBTU) (12 mM, 1.2 equiv). The solution was stirred at RT under argon for 30 min. Then, the amine-functionalized dye (amine CF594) dissolved in 200 µL of anhydrous DMF with a concentration of 11 mM was added to the reaction mixture. To activate the coupling reaction, 2 µL of triethylamine (1.2 µmol, 1.2 equiv) was added to the solution and stirred for 4 h. To quench the reaction, the reaction mixture was directly dried under high vacuum for 2 h. The mixture was diluted with 300 µL of methanol, and 5 µL of solution was injected into LC/MS (Agilent 1200, USA) with a gradient reversed phase system (10 to 100% ACN/H₂O with 0.1% formic acid for 20 min) using Phenomenex Luna 5 µm C₁₈(2) column (100 × 4.6 mm, flow rate; 0.7 mL/min, monitoring of absorption; 254, 320, and 600 nm). The labeled MPA product (MPA*) was purified by reversed phase HPLC (Phenomenex Luna 5 µm C₁₈(2) column of 250 × 10.0 mm, flow rate; 2 mL/min, monitoring of absorption; 254, 320, and 600 nm) with a gradient solvent system (15% to 75% ACN/H₂O with 0.1% formic acid for 40 min).

Cell Line and Mice. HUVEC (CRL-1730) were purchased from ATCC. C57BL/6J (JAX#000664) and B6(C)-H2-Ab1^{bm12}/KhEgJ (BM12, JAX#001162) were obtained from Jackson Laboratory. Male or female mice were used at 7–8 weeks of age and were housed in sterilized and ventilated cages in a specific pathogen-free animal facility under a standard 12 h light/12 h dark cycle. Mice were fed irradiated food and water *ad libitum*. Each individual experiment was performed using three to four mice per group. All animal experiments and methods were performed in accordance with the relevant guidelines and regulations approved by the Institutional Animal Care and Use Committee of Brigham and Women's Hospital, Boston, MA.

Mouse Heterotopic Cardiac Transplantation. Vascularized intra-abdominal heterotopic transplantation of heart allografts was performed using microsurgical techniques.^{24,25} One milliliter of cold heparin (BD Vacutainer sodium heparin #366480, 143USP units/10 mL) was infused into the inferior vena cava (IVC) of the donor mouse. After heparin perfusion, either PBS (control), free MMF, or MMF-NP was infused into the heart from the IVC. The heart was harvested following ligation/dissection of the superior vena cava (SVC) and IVC, and dissection of ascending aorta and pulmonary artery. Harvested donor heart was stored at 4 °C and immersed in UW (University of Wisconsin) solution for 2 h. After abdominal incision of recipient

mouse, abdominal aorta and IVC were clamped. Ascending aorta and pulmonary artery of donor heart were sutured to abdominal aorta and IVC of recipient mouse, respectively, using 10–0 suture. Beating of transplanted heart was observed upon removal of cross clamp, and abdominal incision was closed by 6–0 suture. The survival of cardiac allografts was assessed by daily palpation.

Immunohistochemistry and immunofluorescence. Heart grafts harvested at designated time points post-transplantation were fixed in formalin and embedded in a paraffin block, or they were preserved in Optimal Cutting Temperature (OCT) compound (Tissue-Tek, Torrance, CA) and stored at –80 °C. Samples were cut into 5 µm sections and stained either with H&E (paraffin block section) or with DAPI, anti-F-actin, anti-CD31, anti-CD3, anti-CD11b, fibronectin, VCAM, ICAM, and P-selectin for immunofluorescence (OCT block section).

Histological Assessment of the Allograft Heart. Histological evaluation from H&E slides was done using a score modified from the International Society for Heart and Lung Transplantation.^{95,96} Cellular infiltration was graded blindly from 0 to 4 from 6 random microscopic fields of each heart section (3 sections/heart, 4 mice per group). The grades were defined as follows: grade 0 (no cellular infiltration), grade 1 (less than 25% cellular infiltration), grade 2 (25 to 50% cellular infiltration), grade 3 (50 to 75% cellular infiltration), and grade 4 (more than 75% cellular infiltration with hemorrhage and/or fibrosis). Vascular appearance was determined by a combination of vascular occlusion score and perivascular cellular infiltration. Vascular (artery) occlusion was scored from grade 0 to 3 for every artery (3 sections/heart, 4 mice per group). The grades were defined as follows: grade 0 (no or minimal occlusion, < 10%), grade 1 (10–25% occlusion), grade 2 (25% to 75% occlusion), and grade 3 (more than 75% occlusion). The perivascular cellular infiltration was scored as follows: grade 0 (no cellular infiltration around artery), grade 1 (less than 25% cellular infiltration around artery), grade 2 (25% to 75% cellular infiltration around artery), and grade 3 (more than 75% cellular infiltration around artery). Then, the sum of the vascular occlusion score and perivascular cellular infiltration score was designated as the vascular appearance score.

Flow Cytometry. Flow cytometric analysis was performed of spleen and DLN, and each leukocyte population was quantified. All antibodies were purchased from BD (Becton Dickinson, Franklin Lakes, NJ). Cells were run on a FACS Canto II (BD Bioscience, Franklin Lakes, NJ) instrument. Data were analyzed by using FlowJo software.

DSA Assay. The level of circulating DSA-IgG in recipient mice serum were assessed by flow cytometry. Recipient serum were incubated with donor splenocytes at 37 °C for 30 min, washed, and incubated with FITC-conjugated goat antibody specific for the Fc portion of mouse IgG (Fc blocking antibody) at 4 °C for 1 h. After being stained, the cells were washed, fixed in PBS containing 1% formalin, and analyzed by flow cytometry as mean fluorescence intensity to reflect individual serum DSA-IgG levels.

HUVEC Gene Expression Assessment. HUVEC were stimulated by TNFα (10 ng/mL) and cultured in 6-well plates overnight (0.5 × 10⁶ cells/mL). Either PBS, free MMF, or MMF-NPs were added to the HUVEC at concentrations similar to what was used *in vivo*. The samples were incubated in a humidified 37 °C, 5% CO₂ incubator in triplicates for 24 h. Cells were washed three times with PBS, and the cell suspension was analyzed by qPCR.

Elispot Assay. We followed the manufacturer's instructions (BD Biosciences). Immunospot plates (Millipore) were coated with IFNγ primary antibody for 3 h at 37 °C. Donor (BM12) splenocytes were irradiated at 3000 rads and plated with recipients' (C57BL/6) splenocytes in a 1:1 ratio and incubated in 37 °C for 24 h. Cells were washed out, and the secondary antibody was added and incubated overnight. After development with the chromogen, the total number of spots per well were quantified using an ImmunoSpot Analyzer (Cellular Technology, Cleveland, OH, USA).

Mixed Lymphocyte Reaction Assay. Irradiated donor (BM12) splenocyte stimulators and recipient (C57BL/6) splenocyte responders were added to each well in a 96-well round-bottom plate and incubated at 37 °C for 2 days. An amount of 1 µCi of tritiated thymidine (³H) was

added, and the plate was incubated for additional 14 h. The plate was run on cell Harvester96, TOMTEC.

Quantitative PCR (qPCR). RNA was isolated with TRIZOL (Invitrogen), and cDNA was synthesized using 2 μ g of RNA and high-capacity reverse transcriptase (Invitrogen). RT-PCR was performed with SYBR Green PCR reagents on a Biorad detection system. RNA levels were normalized to the level of GAPDH and calculated as delta–delta threshold cycle ($\Delta\Delta$ CT). Primers used for RT-PCR are listed as follows: GAPDH-F: GTTGTCTCTGCGACTTCA, GAPDH-R: GGTGGTCCAGGGTTTCTTA; IL2-F: TGAGCAGGATGGAGA-ATTACAGG, IL2-R: GTCCAAGTTCATCTTCTAGGCAC, IL6-F: CTCTGGGAAATCGTGGAAAT, IL6-R: CCAGTTTGGTAG-CATCCATC, TNF α -F: ATGAGAAGTTCCCAAATGGC, TNF α -R: CTCCACTTGGTGGTTTGCTA, IFN γ -F: TTGAGGTCAACAAC-CCACAG, IFN γ -R: TCAGCAGCGACTCCTTTTTC, IL17-F: AAGGCAGCAGCGATCATCC, IL17-R: GGAACGGTTGAGGTA-GTCTGAG, CCL2-F: GAAGGAATGGGTCCAGACAT, CCL2-R: ACGGGTCAACTTCACATTCA, CCR2-F: ACACCCTGTTTCGC-TGTAGG, CCR2-R: GATTCCTGGAAGGTGGTCAA, CCL5-F: AGATCTCTGCAGCTGCCCTCA, CCL5-R: GGAGCAC-TTGCTGCTGGTGTAG, CCR5-F: GCTGCCTAAACCCCT-GTCATC, CCR5-R: GTTCTCCTGTGGATCGGGTA, CXCL9-F: CCGAGGCACGATCCACTAC, CXCL9-R: AGGCAGTTTGTAT-CTCCGTT, CXCL10-F: CAAGTGCTGCCGTCATTTTCT, CXCL10-R: ATAGGCTCGCAGGGATGATT, CXCR3-F: TACCTTGAGGTTAGTGAACGTCA, CXCR3-R: CGCTCTC-GTTTTCCCATAATC. VCAM-F: GTCAAAGAACTAC-AAGTCTA, VCAM-R: CTTTATTATCTAACTTCCCTG, ICAM-F: GCAGTGACTCTGTGTGAC, ICAM-R: GGATCTGGTCC-GCTAGCTC, P-selectin-F: TCGGTACCTTGACGTACC, P-selectin-R: CATGGATCCATTCTCAGG, hu-VCAM-F: CTACGCT-GACAATGAATCCTG, hu-VCAM-R: GCAACTGAACACT-TGACTGTG, hu-ICAM-F: CGTGACTGGACTCCAGA, hu-ICAM-R: CACCGTGGTCTGTGACCTC, hu-P-selectin-F: GCAGTGACGGGTACCAAG, hu-P-selectin-R: TGCAGC-TAGACTGATGCTG. All RT-PCR reactions were performed in triplicate.

Statistics. Data analysis was performed by using GraphPad Prism (GraphPad Software, Inc., San Diego, CA). Differences between groups were evaluated by ANOVA to determine significance. Degrees of significance were designated as * $p < 0.05$, ** $p < 0.01$, and *** $p < 0.001$.

Data Availability. All data generated or analyzed during this study are available from the corresponding author on reasonable request.

ASSOCIATED CONTENT

Supporting Information

The Supporting Information is available free of charge on the ACS Publications website at DOI: 10.1021/acsnano.9b05115.

Figure S1 and captions, describing perfusion of donor heart with MMF-NP had no effect on the alloimmune response in the spleen and DLN (PDF)

AUTHOR INFORMATION

Corresponding Authors

*E-mail: mmcgrath8@bwh.harvard.edu. Tel: 617-732-5259. Fax: 617-732-5254.

*E-mail: rabdi@rics.bwh.harvard.edu. Tel: 617-732-5259. Fax: 617-732-5254.

ORCID

Nasim Annabi: 0000-0003-1879-1202

Reza Abdi: 0000-0003-4789-5422

Author Contributions

¹M.U., B.B., and L.J. are co-first authors and contributed equally to this work. M.U. performed microsurgery, performed experiments, analyzed and interpreted data, created images for Figures 1D and 3B, and drafted the manuscript. B.B. synthesized

nanoparticles, performed experiments, immunofluorescence staining, analyzed and interpreted data, and drafted the manuscript. L.J. performed immunofluorescence staining, qPCR experiments, and analyzed and interpreted data. S.J. designed, synthesized MPA*-NP, and performed experiments. V.K. performed experiments and edited the manuscript. N.B. performed experiments and analyzed data. Z.S, Z.J., and F.O. helped experiments. M.B. helped to synthesize MPA*-NP and performed experiments. N.A. helped and advised study regarding to nanoparticle. M.M. and R.A. designed the study, interpreted data, and critically revised and finalized the manuscript.

Notes

The authors declare no competing financial interest.

ACKNOWLEDGMENTS

This work is supported by the National Institutes of Health (NIH) under Award Numbers RO1AI1296596, RO1HL141815, and RO1HL145813 (R.A.) and Brigham Research Institute Stepping Strong Innovator Award (R.A.) and BWH Health & Technology Innovation Fund (R.A.).

REFERENCES

- (1) Ojo, A. O.; Hanson, J. A.; Wolfe, R. A.; Leichtman, A. B.; Agodoa, L. Y.; Port, F. K. Long-Term Survival in Renal Transplant Recipients with Graft Function. *Kidney Int.* **2000**, *57*, 307–313.
- (2) Prakash, J.; Ghosh, B.; Singh, S.; Soni, A.; Rathore, S. S. Causes of Death in Renal Transplant Recipients with Functioning Allograft. *Indian J. Nephrol* **2012**, *22*, 264–268.
- (3) Bamoulid, J.; Staeck, O.; Halleck, F.; Khadzhyov, D.; Brakemeier, S.; Durr, M.; Budde, K. The Need for Minimization Strategies: Current Problems of Immunosuppression. *Transplant Int.* **2015**, *28*, 891–900.
- (4) Vincenti, F.; Friman, S.; Scheuermann, E.; Rostaing, L.; Jenssen, T.; Campistol, J. M.; Uchida, K.; Pescovitz, M. D.; Marchetti, P.; Tuncer, M.; Citterio, F.; Wiecek, A.; Chadban, S.; El-Shahawy, M.; Budde, K.; Goto, N. Results of an International, Randomized Trial Comparing Glucose Metabolism Disorders and Outcome with Cyclosporine Versus Tacrolimus. *Am. J. Transplant.* **2007**, *7*, 1506–1514.
- (5) Silva, H. T., Jr.; Yang, H. C.; Meier-Kriesche, H. U.; Croy, R.; Holman, J.; Fitzsimmons, W. E.; First, M. R. Long-Term Follow-up of a Phase III Clinical Trial Comparing Tacrolimus Extended-Release/Mmf, Tacrolimus/Mmf, and Cyclosporine/Mmf in De Novo Kidney Transplant Recipients. *Transplantation* **2014**, *97*, 636–641.
- (6) Haller, M.; Oberbauer, R. Calcineurin Inhibitor Minimization, Withdrawal and Avoidance Protocols after Kidney Transplantation. *Transplant Int.* **2009**, *22*, 69–77.
- (7) Srinivas, T. R.; Meier-Kriesche, H. U. Minimizing Immunosuppression, an Alternative Approach to Reducing Side Effects: Objectives and Interim Result. *Clin. J. Am. Soc. Nephrol.* **2008**, *3*, S101–S116.
- (8) Dean, P. G.; Park, W. D.; Cornell, L. D.; Schinstock, C. A.; Stegall, M. D. Early Subclinical Inflammation Correlates with Outcomes in Positive Crossmatch Kidney Allografts. *Clin. Transplant.* **2016**, *30*, 925–933.
- (9) van Besouw, N. M.; Caliskan, K.; Peeters, A. M.; Klepper, M.; Dieterich, M.; Maat, L. P.; Weimar, W.; Manintveld, O. C.; Baan, C. C. Interleukin-17-Producing Cd4(+) Cells Home to the Graft Early after Human Heart Transplantation. *J. Heart Lung Transplant* **2015**, *34*, 933–940.
- (10) Weiss, S.; Kotsch, K.; Francuski, M.; Reutzel-Selke, A.; Mantouvalou, L.; Klemz, R.; Kuecuk, O.; Jonas, S.; Wesslau, C.; Ulrich, F.; Pascher, A.; Volk, H. D.; Tullius, S. G.; Neuhaus, P.; Pratschke, J. Brain Death Activates Donor Organs and Is Associated with a Worse I/R Injury after Liver Transplantation. *Am. J. Transplant.* **2007**, *7*, 1584–1593.

- (11) Uehara, M.; Solhjou, Z.; Banouni, N.; Kasinath, V.; Xiaqun, Y.; Dai, L.; Yilmam, O.; Yilmaz, M.; Ichimura, T.; Fiorina, P.; Martins, P. N.; Otori, S.; Guleria, I.; Maarouf, O. H.; Tullius, S. G.; McGrath, M. M.; Abdi, R. Ischemia Augments Alloimmune Injury through Il-6-Driven Cd4(+) Alloreactivity. *Sci. Rep.* **2018**, *8*, 2461.
- (12) Solhjou, Z.; Uehara, M.; Bahmani, B.; Maarouf, O. H.; Ichimura, T.; Brooks, C. R.; Xu, W.; Yilmaz, M.; Elkhali, A.; Tullius, S. G.; Guleria, I.; McGrath, M. M.; Abdi, R. Novel Application of Localized Nanodelivery of Anti-Interleukin-6 Protects Organ Transplant from Ischemia-Reperfusion Injuries. *Am. J. Transplant.* **2017**, *17*, 2326–2337.
- (13) Jurewicz, M.; Ueno, T.; Azzi, J.; Tanaka, K.; Murayama, T.; Yang, S.; Sayegh, M. H.; Niimi, M.; Abdi, R. Donor Antioxidant Strategy Prolongs Cardiac Allograft Survival by Attenuating Tissue Dendritic Cell Immunogenicity(Dagger). *Am. J. Transplant.* **2011**, *11*, 348–355.
- (14) Tran, S.; DeGiovanni, P. J.; Piel, B.; Rai, P. Cancer Nanomedicine: A Review of Recent Success in Drug Delivery. *Clin Transl Med.* **2017**, *6*, 44.
- (15) Shi, J.; Kantoff, P. W.; Wooster, R.; Farokhzad, O. C. Cancer Nanomedicine: Progress, Challenges and Opportunities. *Nat. Rev. Cancer* **2017**, *17*, 20–37.
- (16) Kamaly, N.; Xiao, Z.; Valencia, P. M.; Radovic-Moreno, A. F.; Farokhzad, O. C. Targeted Polymeric Therapeutic Nanoparticles: Design, Development and Clinical Translation. *Chem. Soc. Rev.* **2012**, *41*, 2971–3010.
- (17) Shi, J.; Xiao, Z.; Kamaly, N.; Farokhzad, O. C. Self-Assembled Targeted Nanoparticles: Evolution of Technologies and Bench to Bedside Translation. *Acc. Chem. Res.* **2011**, *44*, 1123–1134.
- (18) Farokhzad, O. C. Nanotechnology for Drug Delivery: The Perfect Partnership. *Expert Opin. Drug Delivery* **2008**, *5*, 927–929.
- (19) Farokhzad, O. C.; Langer, R. Impact of Nanotechnology on Drug Delivery. *ACS Nano* **2009**, *3*, 16–20.
- (20) Ferrari, M. Cancer Nanotechnology: Opportunities and Challenges. *Nat. Rev. Cancer* **2005**, *5*, 161–171.
- (21) Heemann, U.; Kliem, V.; Budde, K.; Hamza, A.; Jurgensen, J. S.; Juarez, F.; Arns, W.; Rath, T.; Haller, H. Mycophenolate Mofetil Maintenance Therapy in Renal Transplant Patients: Long-Term Results of the Trancept Stay Study. *Clin. Transplant.* **2012**, *26*, 919–926.
- (22) Cui, J.; Qin, L.; Zhang, J.; Abrahami, P.; Li, H.; Li, G.; Tietjen, G. T.; Tellides, G.; Pober, J. S.; Mark Saltzman, W. Ex Vivo Pretreatment of Human Vessels with Sirna Nanoparticles Provides Protein Silencing in Endothelial Cells. *Nat. Commun.* **2017**, *8*, 191.
- (23) Tietjen, G. T.; Hosgood, S. A.; DiRito, J.; Cui, J.; Deep, D.; Song, E.; Kraehling, J. R.; Piotrowski-Daspit, A. S.; Kirkiles-Smith, N. C.; Al-Lamki, R.; Thiru, S.; Bradley, J. A.; Saeb-Parsy, K.; Bradley, J. R.; Nicholson, M. L.; Saltzman, W. M.; Pober, J. S. Nanoparticle Targeting to the Endothelium During Normothermic Machine Perfusion of Human Kidneys. *Sci. Transl. Med.* **2017**, *9*, eaam6764.
- (24) Bahmani, B.; Uehara, M.; Jiang, L.; Ordikhani, F.; Banouni, N.; Ichimura, T.; Solhjou, Z.; Furtmuller, G. J.; Brandacher, G.; Alvarez, D.; von Andrian, U. H.; Uchimura, K.; Xu, Q.; Vohra, I.; Yilmam, O. A.; Haik, Y.; Azzi, J.; Kasinath, V.; Bromberg, J. S.; McGrath, M. M.; Abdi, R. Targeted Delivery of Immune Therapeutics to Lymph Nodes Prolongs Cardiac Allograft Survival. *J. Clin. Invest.* **2018**, *128*, 4770–4786.
- (25) Corry, R. J.; Winn, H. J.; Russell, P. S. Heart Transplantation in Congenic Strains of Mice. *Transplant Proc.* **1973**, *5*, 733–735.
- (26) Khosroshahi, H. T.; Shoja, M. M.; Peyrovifar, A.; Hashemi, S. R.; Amjadi, M. Mycophenolate Mofetil Dose Reduction in Renal Transplant Recipients: A 5-Year Follow-up Study. *Transplant. Proc.* **2009**, *41*, 2797–2799.
- (27) Jorge, S.; Guerra, J.; Santana, A.; Mil-Homens, C.; Prata, M. M. Mycophenolate Mofetil: Ten Years' Experience of a Renal Transplant Unit. *Transplant. Proc.* **2008**, *40*, 700–704.
- (28) Manito, N.; Rabago, G.; Palomo, J.; Arizon, J. M.; Delgado, J.; Almenar, L.; Crespo-Leiro, M. G.; Lage, E.; Pulpon, L. Improvement in Chronic Renal Failure after Mycophenolate Mofetil Introduction and Cyclosporine Dose Reduction: Four-Year Results from a Cohort of Heart Transplant Recipients. *Transplant. Proc.* **2011**, *43*, 2699–2706.
- (29) Allison, A. C.; Eugui, E. M. Mechanisms of Action of Mycophenolate Mofetil in Preventing Acute and Chronic Allograft Rejection. *Transplantation* **2005**, *80*, S181–190.
- (30) Klupp, J.; Dambrin, C.; Hibi, K.; Luna, J.; Suzuki, T.; Hausen, B.; Birsan, T.; Van Gelder, T.; Fitzgerald, P. J.; Berry, G.; Morris, R. E. Treatment by Mycophenolate Mofetil of Advanced Graft Vascular Disease in Non-Human Primate Recipients of Orthotopic Aortic Allografts. *Am. J. Transplant.* **2003**, *3*, 817–829.
- (31) Racusen, L. C.; Regele, H. The Pathology of Chronic Allograft Dysfunction. *Kidney Int.* **2010**, *78*, S27–32.
- (32) Chapman, J. R.; O'Connell, P. J.; Nankivell, B. J. Chronic Renal Allograft Dysfunction. *J. Am. Soc. Nephrol.* **2005**, *16*, 3015–3026.
- (33) Merola, J.; Jane-Wit, D. D.; Pober, J. S. Recent Advances in Allograft Vasculopathy. *Curr. Opin. Organ Transplant.* **2017**, *22*, 1–7.
- (34) Okada, M.; Wang, C. Y.; Hwang, D. W.; Sakaguchi, T.; Olson, K. E.; Yoshikawa, Y.; Minamoto, K.; Mazer, S. P.; Yan, S. F.; Pinsky, D. J. Transcriptional Control of Cardiac Allograft Vasculopathy by Early Growth Response Gene-1 (Egr-1). *Circ. Res.* **2002**, *91*, 135–142.
- (35) Vincenti, F. Immunosuppression Minimization: Current and Future Trends in Transplant Immunosuppression. *J. Am. Soc. Nephrol.* **2003**, *14*, 1940–1948.
- (36) Naesens, M.; Kuypers, D. R.; Sarwal, M. Calcineurin Inhibitor Nephrotoxicity. *Clin. J. Am. Soc. Nephrol.* **2009**, *4*, 481–508.
- (37) Vincenti, F.; Larsen, C.; Durrbach, A.; Wekerle, T.; Nashan, B.; Blacho, G.; Lang, P.; Grinyo, J.; Halloran, P. F.; Solez, K.; Hagerty, D.; Levy, E.; Zhou, W.; Natarajan, K.; Charpentier, B. Belatacept Study G. Costimulation Blockade with Belatacept in Renal Transplantation. *N. Engl. J. Med.* **2005**, *353*, 770–781.
- (38) Meier-Kriesche, H. U.; Baliga, R.; Kaplan, B. Decreased Renal Function Is a Strong Risk Factor for Cardiovascular Death after Renal Transplantation. *Transplantation* **2003**, *75*, 1291–1295.
- (39) Halloran, P. F. Immunosuppressive Drugs for Kidney Transplantation. *N. Engl. J. Med.* **2004**, *351*, 2715–2729.
- (40) Naesens, M.; Lerut, E.; Sarwal, M.; Van Damme, B.; Vanrenterghem, Y.; Kuypers, D. R. Balancing Efficacy and Toxicity of Kidney Transplant Immunosuppression. *Transplant. Proc.* **2009**, *41*, 3393–3395.
- (41) Gelman, A. E.; Li, W.; Richardson, S. B.; Zinselmeyer, B. H.; Lai, J.; Okazaki, M.; Kornfeld, C. G.; Kreisel, F. H.; Sugimoto, S.; Tietjen, J. R.; Dempster, J.; Patterson, G. A.; Krupnick, A. S.; Miller, M. J.; Kreisel, D. Cutting Edge: Acute Lung Allograft Rejection Is Independent of Secondary Lymphoid Organs. *J. Immunol.* **2009**, *182*, 3969–3973.
- (42) Asaoka, T.; Marubashi, S.; Kobayashi, S.; Hama, N.; Eguchi, H.; Takeda, Y.; Tanemura, M.; Wada, H.; Takemasa, I.; Takahashi, H.; Ruiz, P.; Doki, Y.; Mori, M.; Nagano, H. Intra-graft Transcriptome Level of Cxcl9 as Biomarker of Acute Cellular Rejection after Liver Transplantation. *J. Surg. Res.* **2012**, *178*, 1003–1014.
- (43) Solhjou, Z.; Athar, H.; Xu, Q.; Abdi, R. Emerging Therapies Targeting Intra-Organ Inflammation in Transplantation. *Am. J. Transplant.* **2015**, *15*, 305–311.
- (44) Enk, A. H.; Angeloni, V. L.; Udey, M. C.; Katz, S. I. An Essential Role for Langerhans Cell-Derived Il-1 Beta in the Initiation of Primary Immune Responses in Skin. *J. Immunol.* **1993**, *150*, 3698–3704.
- (45) Steinman, R. M.; Inaba, K.; Turley, S.; Pierre, P.; Mellman, I. Antigen Capture, Processing, and Presentation by Dendritic Cells: Recent Cell Biological Studies. *Hum. Immunol.* **1999**, *60*, S62–S67.
- (46) Kimber, I.; Cumberbatch, M. Stimulation of Langerhans Cell Migration by Tumor Necrosis Factor Alpha (Tnf-Alpha). *J. Invest. Dermatol.* **1992**, *99*, S48–S50.
- (47) Jurewicz, M.; Takakura, A.; Augello, A.; Naini, S. M.; Ichimura, T.; Zandi-Nejad, K.; Abdi, R. Ischemic Injury Enhances Dendritic Cell Immunogenicity Via Tlr4 and Nf-Kappa B Activation. *J. Immunol.* **2010**, *184*, 2939–2948.
- (48) Batal, I.; Azzi, J.; Mounayar, M.; Abdoli, R.; Moore, R.; Lee, J. Y.; Rosetti, F.; Wang, C.; Fiorina, P.; Sackstein, R.; Ichimura, T.; Abdi, R. The Mechanisms of up-Regulation of Dendritic Cell Activity by Oxidative Stress. *J. Leukocyte Biol.* **2014**, *96*, 283–293.

- (49) Ingulli, E. Mechanism of Cellular Rejection in Transplantation. *Pediatr. Nephrol.* **2010**, *25*, 61–74.
- (50) Golshayan, D.; Lechler, R. Commentary: Priming of Alloreactive T Cells—Where Does It Happen? *Eur. J. Immunol.* **2004**, *34*, 3301–3304.
- (51) Su, C. A.; Iida, S.; Abe, T.; Fairchild, R. L. Endogenous Memory Cd8 T Cells Directly Mediate Cardiac Allograft Rejection. *Am. J. Transplant.* **2014**, *14*, 568–579.
- (52) El-Sawy, T.; Miura, M.; Fairchild, R. Early T Cell Response to Allografts Occurring Prior to Alloantigen Priming up-Regulates Innate-Mediated Inflammation and Graft Necrosis. *Am. J. Pathol.* **2004**, *165*, 147–157.
- (53) Valujskikh, A.; Heeger, P. S. Emerging Roles of Endothelial Cells in Transplant Rejection. *Curr. Opin. Immunol.* **2003**, *15*, 493–498.
- (54) Biedermann, B. C.; Pober, J. S. Human Endothelial Cells Induce and Regulate Cytolytic T Cell Differentiation. *J. Immunol.* **1998**, *161*, 4679–4687.
- (55) Briscoe, D. M.; Alexander, S. I.; Lichtman, A. H. Interactions between T Lymphocytes and Endothelial Cells in Allograft Rejection. *Curr. Opin. Immunol.* **1998**, *10*, 525–531.
- (56) Briscoe, D. M.; Henault, L. E.; Geehan, C.; Alexander, S. I.; Lichtman, A. H. Human Endothelial Cell Costimulation of T Cell Ifn- γ Production. *J. Immunol.* **1997**, *159*, 3247–3256.
- (57) Marelli-Berg, F. M.; Scott, D.; Bartok, I.; Peek, E.; Dyson, J.; Lechler, R. I. Activated Murine Endothelial Cells Have Reduced Immunogenicity for Cd8+ T Cells: A Mechanism of Immunoregulation? *J. Immunol.* **2000**, *165*, 4182–4189.
- (58) Marelli-Berg, F. M.; Scott, D.; Bartok, I.; Peek, E.; Dyson, J.; Lechler, R. I. Antigen Presentation by Murine Endothelial Cells. *Transplant. Proc.* **2001**, *33*, 315–316.
- (59) Herrera, O. B.; Golshayan, D.; Tibbott, R.; Salcido Ochoa, F.; James, M. J.; Marelli-Berg, F. M.; Lechler, R. I. A Novel Pathway of Alloantigen Presentation by Dendritic Cells. *J. Immunol.* **2004**, *173*, 4828–4837.
- (60) Manes, T. D.; Pober, J. S. Antigen Presentation by Human Microvascular Endothelial Cells Triggers Icam-1-Dependent Transendothelial Protrusion by, and Fractalkine-Dependent Transendothelial Migration of, Effector Memory Cd4+ T Cells. *J. Immunol.* **2008**, *180*, 8386–8392.
- (61) Pober, J. S.; Kluger, M. S.; Schechner, J. S. Human Endothelial Cell Presentation of Antigen and the Homing of Memory/Effector T Cells to Skin. *Ann. N. Y. Acad. Sci.* **2001**, *941*, 12–25.
- (62) Pober, J. S.; Merola, J.; Liu, R.; Manes, T. D. Antigen Presentation by Vascular Cells. *Front. Immunol.* **2017**, *8*, 1907.
- (63) Denton, M. D.; Geehan, C. S.; Alexander, S. I.; Sayegh, M. H.; Briscoe, D. M. Endothelial Cells Modify the Costimulatory Capacity of Transmigrating Leukocytes and Promote Cd28-Mediated Cd4+ T Cell Alloactivation. *J. Exp. Med.* **1999**, *190*, 555–566.
- (64) Denton, M. D.; Geehan, C. S.; Alexander, S. I.; Sayegh, M. H.; Briscoe, D. M. Endothelial Cells Modify the Costimulatory Capacity of Transmigrating Leukocytes and Promote Cd28-Mediated Cd4(+) T Cell Alloactivation. *J. Exp. Med.* **1999**, *190*, 555–566.
- (65) Tietjen, G. T.; Bracaglia, L. G.; Saltzman, W. M.; Pober, J. S. Focus on Fundamentals: Achieving Effective Nanoparticle Targeting. *Trends Mol. Med.* **2018**, *24*, 598–606.
- (66) Shimizu, H.; Takahashi, M.; Takeda, S.; Inoue, S.; Fujishiro, J.; Hakamata, Y.; Kaneko, T.; Murakami, T.; Takeuchi, K.; Takeyoshi, I.; Morishita, Y.; Kobayashi, E. Mycophenolate Mofetil Prevents Transplant Arteriosclerosis by Direct Inhibition of Vascular Smooth Muscle Cell Proliferation. *Transplantation* **2004**, *77*, 1661–1667.
- (67) Allison, A. C.; Hovi, T.; Watts, R. W.; Webster, A. D. The Role of De Novo Purine Synthesis in Lymphocyte Transformation. *Ciba Found Symp.* **2008**, *207*–224.
- (68) Srinivas, T. R.; Kaplan, B.; Schold, J. D.; Meier-Kriesche, H. U. The Impact of Mycophenolate Mofetil on Long-Term Outcomes in Kidney Transplantation. *Transplantation* **2005**, *80*, S211–220.
- (69) Kitchin, J. E.; Pomeranz, M. K.; Pak, G.; Washenik, K.; Shupack, J. L. Rediscovering Mycophenolic Acid: A Review of Its Mechanism, Side Effects, and Potential Uses. *J. Am. Acad. Dermatol.* **1997**, *37*, 445–449.
- (70) Blaheta, R. A.; Leckel, K.; Wittig, B.; Zenker, D.; Oppermann, E.; Harder, S.; Scholz, M.; Weber, S.; Schuldes, H.; Encke, A.; Markus, B. H. Inhibition of Endothelial Receptor Expression and of T-Cell Ligand Activity by Mycophenolate Mofetil. *Transplant Immunol.* **1998**, *6*, 251–259.
- (71) Glomsda, B. A.; Blaheta, R. A.; Hailer, N. P. Inhibition of Monocyte/Endothelial Cell Interactions and Monocyte Adhesion Molecule Expression by the Immunosuppressant Mycophenolate Mofetil. *Spinal Cord* **2003**, *41*, 610–619.
- (72) Hoffmann, J.; Bohm, M.; Abele-Ohl, S.; Ramsperger-Gleixner, M.; Spriewald, B. M.; Zinser, E.; Steinkasserer, A.; Weyand, M.; Ensminger, S. M. Reduction of Transplant Arteriosclerosis after Treatment with Mycophenolate Mofetil and Ganciclovir in a Mouse Aortic Allograft Model. *Exp Clin Transplant* **2012**, *10*, 592–600.
- (73) Devalliere, J.; Chang, W. G.; Andrejcsk, J. W.; Abrahami, P.; Cheng, C. J.; Jane-Wit, D.; Saltzman, W. M.; Pober, J. S. Sustained Delivery of Proangiogenic MicroRNA-132 by Nanoparticle Transfection Improves Endothelial Cell Transplantation. *FASEB J.* **2014**, *28*, 908–922.
- (74) Liang, Y.; Christopher, K.; Finn, P. W.; Colson, Y. L.; Perkins, D. L. Graft Produced Interleukin-6 Functions as a Danger Signal and Promotes Rejection after Transplantation. *Transplantation* **2007**, *84*, 771–777.
- (75) Booth, A. J.; Grabauskiene, S.; Wood, S. C.; Lu, G.; Burrell, B. E.; Bishop, D. K. Il-6 Promotes Cardiac Graft Rejection Mediated by Cd4+ Cells. *J. Immunol.* **2011**, *187*, 5764–5771.
- (76) Diaz, J. A.; Booth, A. J.; Lu, G.; Wood, S. C.; Pinsky, D. J.; Bishop, D. K. Critical Role for Il-6 in Hypertrophy and Fibrosis in Chronic Cardiac Allograft Rejection. *Am. J. Transplant.* **2009**, *9*, 1773–1783.
- (77) Zhao, X.; Boenisch, O.; Yeung, M.; Mfarrej, B.; Yang, S.; Turka, L. A.; Sayegh, M. H.; Iacomini, J.; Yuan, X. Critical Role of Proinflammatory Cytokine Il-6 in Allograft Rejection and Tolerance. *Am. J. Transplant.* **2012**, *12*, 90–101.
- (78) Kimura, N.; Itoh, S.; Nakae, S.; Axtell, R. C.; Velotta, J. B.; Bos, E. J.; Merk, D. R.; Gong, Y.; Okamura, H.; Nagamine, C. M.; Adachi, H.; Kornfeld, H.; Robbins, R. C.; Fischbein, M. P. Interleukin-16 Deficiency Suppresses the Development of Chronic Rejection in Murine Cardiac Transplantation Model. *J. Heart Lung Transplant* **2011**, *30*, 1409–1417.
- (79) Fogal, B.; Yi, T.; Wang, C.; Rao, D. A.; Lebastchi, A.; Kulkarni, S.; Tellides, G.; Pober, J. S. Neutralizing Il-6 Reduces Human Arterial Allograft Rejection by Allowing Emergence of Cd161+ Cd4+ Regulatory T Cells. *J. Immunol.* **2011**, *187*, 6268–6280.
- (80) Baggiolini, M. Chemokines and Leukocyte Traffic. *Nature* **1998**, *392*, 565–568.
- (81) Huang, Y.; Liu, Z.; Huang, H.; Liu, H.; Li, L. Effects of Mycophenolic Acid on Endothelial Cells. *Int. Immunopharmacol.* **2005**, *5*, 1029–1039.
- (82) Olejarz, W.; Bryk, D.; Zapolska-Downar, D.; Malecki, M.; Stachurska, A.; Sitkiewicz, D. Mycophenolic Acid Attenuates the Tumour Necrosis Factor-Alpha-Mediated Proinflammatory Response in Endothelial Cells by Blocking the Mapk/Nf-Kappab and Ros Pathways. *Eur. J. Clin. Invest.* **2014**, *44*, 54–64.
- (83) Jane-Wit, D.; Manes, T. D.; Yi, T.; Qin, L.; Clark, P.; Kirkles-Smith, N. C.; Abrahami, P.; Devalliere, J.; Moeckel, G.; Kulkarni, S.; Tellides, G.; Pober, J. S. Alloantibody and Complement Promote T Cell-Mediated Cardiac Allograft Vasculopathy through Noncanonical Nuclear Factor-Kappab Signaling in Endothelial Cells. *Circulation* **2013**, *128*, 2504–2516.
- (84) von Horn, C.; Minor, T. Isolated Kidney Perfusion: The Influence of Pulsatile Flow. *Scand. J. Clin. Lab. Invest.* **2018**, *78*, 131–135.
- (85) Werner, N. L.; Alghanem, F.; Rakestraw, S. L.; Sarver, D. C.; Nicely, B.; Pietroski, R. E.; Lange, P.; Rudich, S. M.; Mendias, C. L.; Rojas-Pena, A.; Magee, J. C.; Bartlett, R. H.; Ozer, K. Ex Situ Perfusion of Human Limb Allografts for 24 h. *Transplantation* **2017**, *101*, e68–e74.

(86) Hosgood, S. A.; Shah, K.; Patel, M.; Nicholson, M. L. The Effect of Prolonged of Warm Ischaemic Injury on Renal Function in an Experimental Ex Vivo Normothermic Perfusion System. *J. Transl. Med.* **2015**, *13*, 207.

(87) Patel, K.; Atkinson, C.; Tran, D.; Nadig, S. N. Nanotechnological Approaches to Immunosuppression and Tolerance Induction. *Curr. Transplant Rep* **2017**, *4*, 159–168.

(88) Zhu, P.; Atkinson, C.; Dixit, S.; Cheng, Q.; Tran, D.; Patel, K.; Jiang, Y. L.; Eskilsen, S.; Miller, K.; Bazzle, G.; Allen, P.; Moore, A.; Broome, A. M.; Nadig, S. N. Organ Preservation with Targeted Rapamycin Nanoparticles: A Pre-Treatment Strategy Preventing Chronic Rejection in Vivo. *RSC Adv.* **2018**, *8*, 25909–25919.

(89) Nadig, S. N.; Dixit, S. K.; Levey, N.; Eskilsen, S.; Miller, K.; Dennis, W.; Atkinson, C.; Broome, A. M. Immunosuppressive Nano-Therapeutic Micelles Downregulate Endothelial Cell Inflammation and Immunogenicity. *RSC Adv.* **2015**, *5*, 43552–43562.

(90) Dong, Y.; Feng, S. S. Poly(D,L-Lactide-Co-Glycolide)/Montmorillonite Nanoparticles for Oral Delivery of Anticancer Drugs. *Biomaterials* **2005**, *26*, 6068–6076.

(91) Kim, D. H.; Martin, D. C. Sustained Release of Dexamethasone from Hydrophilic Matrices Using Plga Nanoparticles for Neural Drug Delivery. *Biomaterials* **2006**, *27*, 3031–3037.

(92) Aguado, M. T.; Lambert, P. H. Controlled-Release Vaccines–Biodegradable Polylactide/Polyglycolide (Pl/Pg) Microspheres as Antigen Vehicles. *Immunobiology* **1992**, *184*, 113–125.

(93) Kelly, R. J. Clinical and Laboratory Evaluation of a New Synthetic Absorbable Suture. *Rev. Surg.* **1970**, *27*, 142–143.

(94) Blanco, E.; Shen, H.; Ferrari, M. Principles of Nanoparticle Design for Overcoming Biological Barriers to Drug Delivery. *Nat. Biotechnol.* **2015**, *33*, 941–951.

(95) Billingham, M. E.; Cary, N. R.; Hammond, M. E.; Kemnitz, J.; Marboe, C.; McCallister, H. A.; Snovar, D. C.; Winters, G. L.; Zerbe, A. A Working Formulation for the Standardization of Nomenclature in the Diagnosis of Heart and Lung Rejection: Heart Rejection Study Group. The International Society for Heart Transplantation. *J. Heart Transplant* **1990**, *9*, 587–593.

(96) Stewart, S.; Winters, G. L.; Fishbein, M. C.; Tazelaar, H. D.; Kobashigawa, J.; Abrams, J.; Andersen, C. B.; Angelini, A.; Berry, G. J.; Burke, M. M.; Demetris, A. J.; Hammond, E.; Itescu, S.; Marboe, C. C.; McManus, B.; Reed, E. F.; Reinsmoen, N. L.; Rodriguez, E. R.; Rose, A. G.; Rose, M.; Suci-Focia, N.; Zeevi, A.; Billingham, M. E. Revision of the 1990 Working Formulation for the Standardization of Nomenclature in the Diagnosis of Heart Rejection. *J. Heart Lung Transplant* **2005**, *24*, 1710–1720.